



HAL
open science

Crystal structure, Hirshfeld surface analysis, inter-action energy and energy framework calculations, as well as density functional theory (DFT) computation, of methyl 2-oxo-1-(prop-2-yn-yl)-1,2-di-hydro-quinoline-4-carboxyl-ate.

A. El-Mrabet, A. Haoudi, S. Dalbouha, M. K. Skalli, T. Hökelek, Frederic Capet, Y. Kandri Rodi, Ahmed Mazzah, N. K. Sebbar

► **To cite this version:**

A. El-Mrabet, A. Haoudi, S. Dalbouha, M. K. Skalli, T. Hökelek, et al.. Crystal structure, Hirshfeld surface analysis, inter-action energy and energy framework calculations, as well as density functional theory (DFT) computation, of methyl 2-oxo-1-(prop-2-yn-yl)-1,2-di-hydro-quinoline-4-carboxyl-ate.. Acta crystallographica Section E: Crystallographic communications [2015-..], 2023, Acta crystallographica Section E: Crystallographic communications [2015-..], 79, pp.883-889. 10.1107/S2056989023007557 . hal-04451945

HAL Id: hal-04451945

<https://hal.univ-lille.fr/hal-04451945>

Submitted on 12 Feb 2024

HAL is a multi-disciplinary open access archive for the deposit and dissemination of scientific research documents, whether they are published or not. The documents may come from teaching and research institutions in France or abroad, or from public or private research centers.

L'archive ouverte pluridisciplinaire **HAL**, est destinée au dépôt et à la diffusion de documents scientifiques de niveau recherche, publiés ou non, émanant des établissements d'enseignement et de recherche français ou étrangers, des laboratoires publics ou privés.



Distributed under a Creative Commons Attribution 4.0 International License

Received 12 July 2023

Accepted 29 August 2023

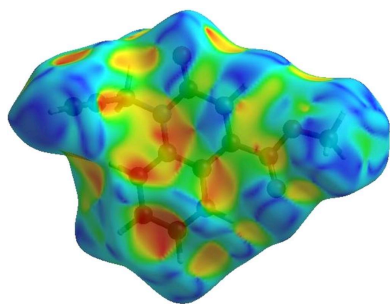
Edited by M. Weil, Vienna University of Technology, Austria

This article is part of a collection of articles to commemorate the founding of the African Crystallographic Association and the 75th anniversary of the IUCr.

Keywords: crystal structure; π -stacking; C—H...O hydrogen bonds; dihydroquinoline.

CCDC reference: 2291603

Supporting information: this article has supporting information at journals.iucr.org/e



Crystal structure, Hirshfeld surface analysis, interaction energy and energy framework calculations, as well as density functional theory (DFT) computation, of methyl 2-oxo-1-(prop-2-ynyl)-1,2-dihydroquinoline-4-carboxylate

Ayoub El-Mrabet,^a Amal Haoudi,^a Samira Dalbouha,^{b,c,*} Mohamed Khalid Skalli,^a Tuncer Hökelek,^d Frederic Capet,^e Youssef Kandri Rodi,^a Ahmed Mazzah^f and Nada Kheira Sebbar^g

^aLaboratory of Applied Organic Chemistry, Faculty of Science and Technology, University of Sidi Mohamed Ben Abdellah, BP 2202, Fez, Morocco, ^bLaboratory of Organic Chemistry and Physical Chemistry, Research Team: Molecular Modeling, Materials and Environment, Department of Chemistry, Faculty of Sciences, University Ibn Zohr in Agadir, BP 8106 Agadir, Morocco, ^cLaboratory of Spectroscopy, Molecular Modeling, Materials, Nanomaterials, Water and Environment, CERNE2D, Faculty of Sciences, Mohammed V University in Rabat, Av. Ibn Battouta, BP 1014, Rabat, Morocco, ^dDepartment of Physics, Hacettepe University, 06800 Beytepe, Ankara, Türkiye, ^eUniversity of Lille, CNRS, UMR 8181, UCCS, Unité de catalyse et Chimie du solide, F-59000 Lille, France, ^fUniversity of Lille, CNRS, UAR 3290, MSAP, Miniaturization for Synthesis, Analysis and Proteomics, F-59000 Lille, France, and ^gLaboratoire de Chimie Bioorganique Appliquée, Faculté des Sciences, Université Ibnou Zohr, Agadir, Morocco. *Correspondence e-mail: samiradalbouha@gmail.com

In the title molecule, C₁₄H₁₁NO₃, the dihydroquinoline core deviates slightly from planarity, indicated by the dihedral angle of 1.07 (3)° between the two six-membered rings. In the crystal, layers of molecules almost parallel to the *bc* plane are formed by C—H...O hydrogen bonds. These are joined by π - π stacking interactions. A Hirshfeld surface analysis revealed that the most important contributions to the crystal packing are from H...H (36.0%), H...C/C...H (28.9%) and H...O/O...H (23.5%) interactions. The evaluation of the electrostatic, dispersion and total energy frameworks indicates that the stabilization is dominated by the dispersion energy contribution. Moreover, the molecular structure optimized by density functional theory (DFT) at the B3LYP/6-311G(d,p) level is compared with the experimentally determined molecular structure in the solid state. The HOMO–LUMO behaviour was elucidated to determine the energy gap.

1. Chemical context

Quinoline derivatives form a class of heterocyclic compounds that have received much attention due to their biological and pharmacological activities (Filali Baba *et al.*, 2019; Hayani *et al.*, 2021). They are used in the pharmaceutical industry because of their antimicrobial (Katoh *et al.*, 2004; Abdel-Wahab *et al.*, 2012), anti-inflammatory (Leatham *et al.*, 1983), antihypertensive (Muruganatham *et al.*, 2004), antibiotic (Mahamoud *et al.*, 2006), anti-HIV (Wilson *et al.*, 1992; Strekowski *et al.*, 1991) and corrosion inhibitive activities (Filali Baba *et al.*, 2016*a,b*). They are also considered as an important scaffold for the development of new pharmaceutically active agents (Filali Baba *et al.*, 2020; Bouzian *et al.*, 2018).

In continuation of our research work devoted to the study of O-alkylation and N-alkylation reactions involving quinoline derivatives, we report herein the synthesis and the molecular and crystal structures of methyl 2-oxo-1-(prop-2-ynyl)-1,2-dihydroquinoline-4-carboxylate, obtained by an alkylation

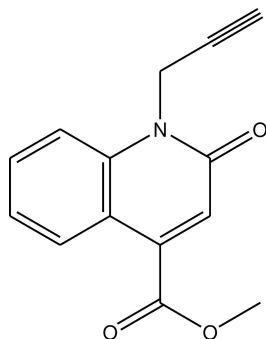
Table 1

Hydrogen-bond geometry (Å, °).

<i>D</i> —H... <i>A</i>	<i>D</i> —H	H... <i>A</i>	<i>D</i> ... <i>A</i>	<i>D</i> —H... <i>A</i>
C9—H9...O3	0.969 (17)	2.210 (15)	2.8807 (19)	125.3 (12)
C10—H10A...O1	0.922 (16)	2.277 (17)	2.6961 (17)	107.1 (12)
C14—H14B...O1 ⁱ	0.95 (2)	2.56 (2)	3.433 (2)	153.8 (18)

Symmetry code: (i) $-x, -y + 1, -z + 1$.

reaction of methyl 2-oxo-1,2-dihydroquinoline-4-carboxylate using an excess of propargyl bromide as an alkylating reagent in phase transfer catalysis (PTC). Moreover, a Hirshfeld surface analysis and interaction energy and energy framework calculations were performed. The molecular structure optimized by density functional theory (DFT) at the B3LYP/6-311G(d,p) level is compared with the experimentally determined molecular structure in the solid state.



2. Structural commentary

The dihydroquinoline core of the title molecule (Fig. 1) deviates slightly from planarity, as indicated by the dihedral angle of 1.07 (3)° between the mean planes of the *A* (C1–C5/N1) and *B* (C4–C9) rings. Atoms O1, O2, O3, C10, C13 and C14 are -0.1294 (11), 0.1907 (12), -0.2708 (15), 0.0177 (14), -0.0267 (13) and 0.0953 (23) Å from the least-squares plane of the *A* ring. The O2–C13 [1.3123 (17) Å] and O3–C13 [1.1955 (16) Å] distances in the ester group indicate localized single and double bonds, rather than delocalized bonding

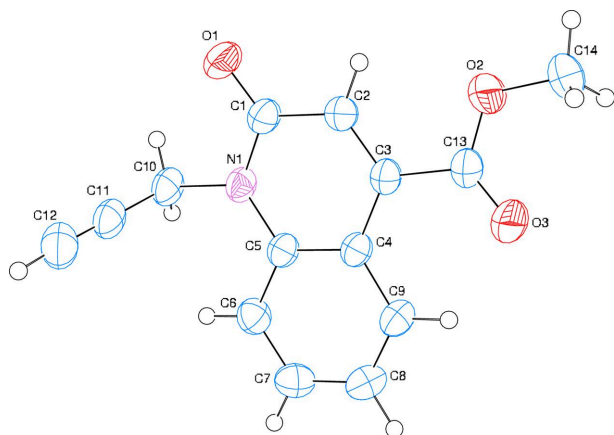


Figure 1

The molecular structure of the title compound with the atom-labeling scheme and displacement ellipsoids drawn at the 50% probability level.

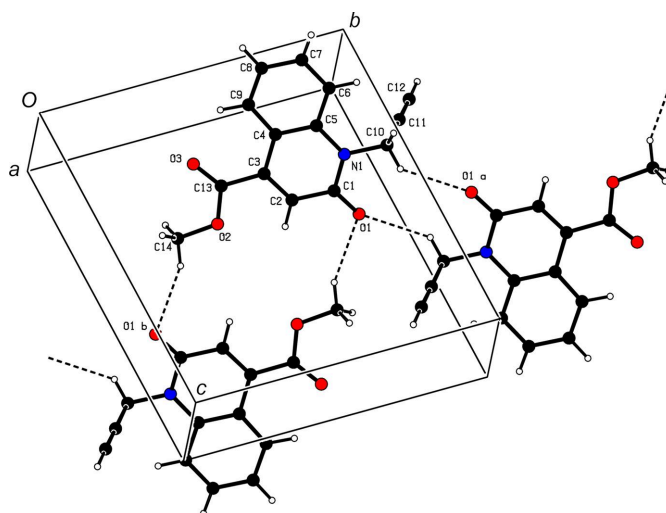


Figure 2

A partial packing diagram, viewed down the *a* axis, with C–H...O hydrogen bonds shown as dashed lines.

arrangements. The O2–C13–O3 bond angle [122.55 (12)°] seems to be slightly increased with respect to that present in a free acid (122.2°; Sim *et al.*, 1955). The O2–C13–O3 bond angle may be compared with the corresponding value of 124.27 (17)° in diaquabis(2-bromobenzoato- κ O)bis(nicotinamide- κ N¹)zinc(II) (Hökelek *et al.*, 2009).

3. Supramolecular features

In the crystal, C–H...O hydrogen bonds (Table 1) link the molecules, enclosing $R_2^2(10)$ and $R_2^2(16)$ ring motifs, into layers almost parallel to the *bc* plane (Fig. 2). These layers are further connected by π – π stacking interactions between the *A* and *B*($x - 1, y, z$) rings [centroid-to-centroid distance = 3.5629 (7) Å, $\alpha = 1.13^\circ$ and slippage = 1.221 Å] to form a triperiodic network.

4. Hirshfeld surface analysis

In order to visualize the intermolecular interactions in the crystal of the title compound, a Hirshfeld surface (HS) analysis (Hirshfeld, 1977) was carried out by using *Crystal-*

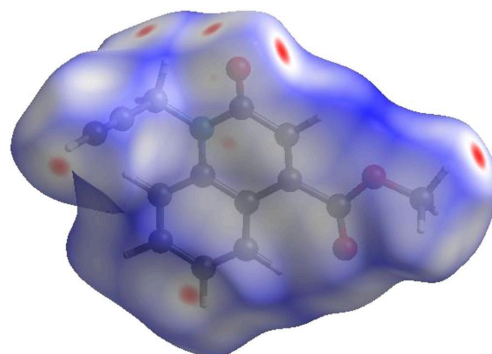


Figure 3

View of the three-dimensional Hirshfeld surface of the title compound, plotted over d_{norm} in the range from -0.1226 to 1.1991 a.u.

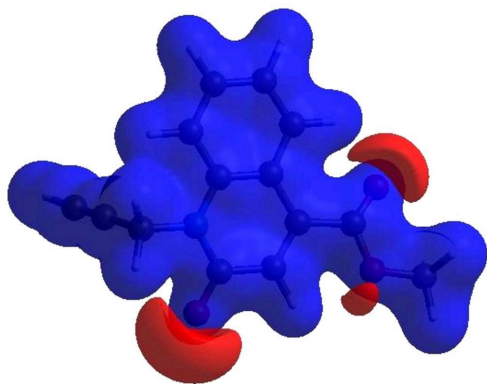


Figure 4
View of the three-dimensional Hirshfeld surface of the title compound plotted over electrostatic potential energy in the range from -0.0500 to 0.0500 a.u., using the STO-3G basis set at the Hartree–Fock level of theory.

Explorer (Spackman *et al.*, 2021). In the HS plotted over d_{norm} (Fig. 3), the white surface indicates contacts with distances equal to the sum of the van der Waals radii, and the red and blue colours indicate distances shorter (in close contact) or

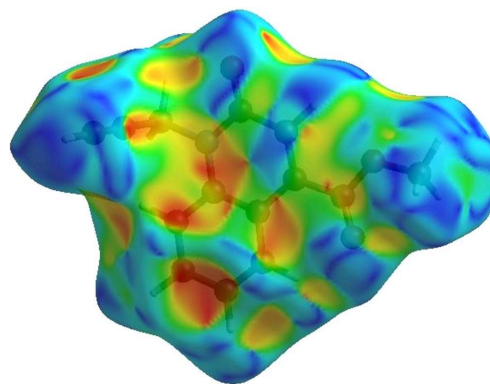


Figure 5
The Hirshfeld surface of the title compound plotted over shape-index.

longer (distinct contact) than the sum of the van der Waals radii (Venkatesan *et al.*, 2016). The bright-red spots indicate their roles as respective donors and/or acceptors; they also appear as blue and red regions corresponding to positive and negative potentials on the HS mapped over electrostatic potential (Spackman *et al.*, 2008; Jayatilaka *et al.*, 2005), as

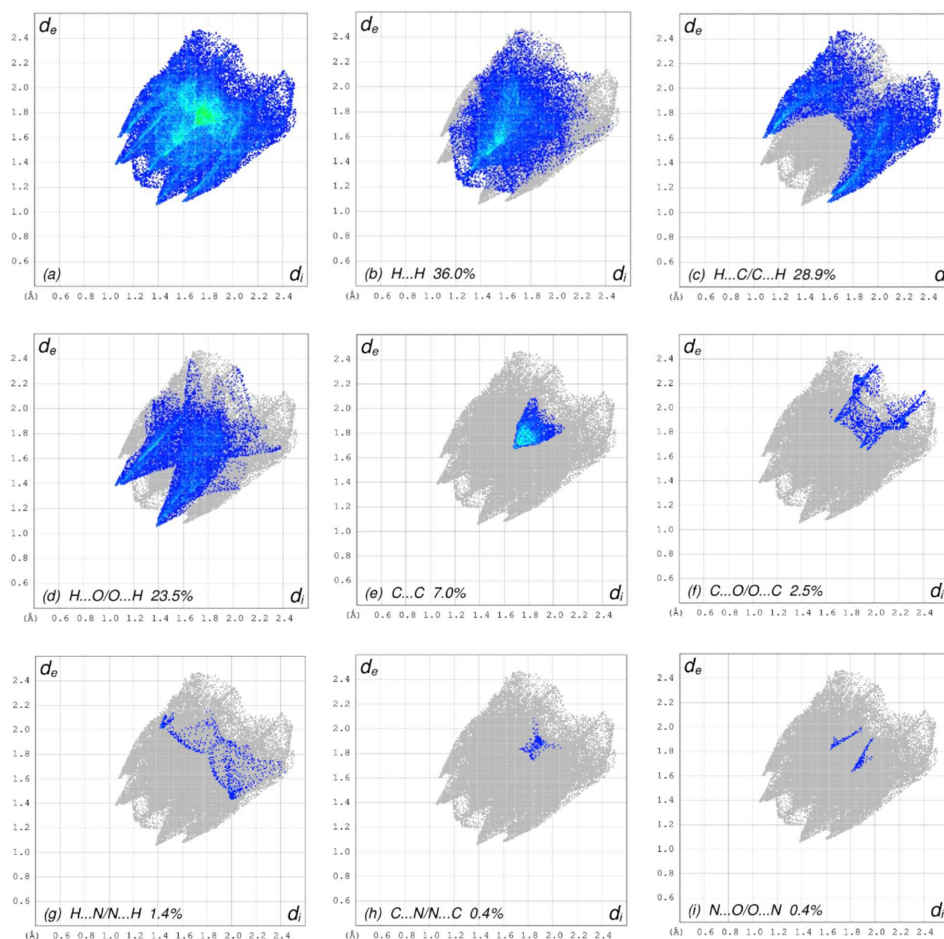


Figure 6
The full two-dimensional fingerprint plots for the title compound, showing (a) all interactions, (b) $\text{H}\cdots\text{H}$, (c) $\text{H}\cdots\text{C}/\text{C}\cdots\text{H}$, (d) $\text{H}\cdots\text{O}/\text{O}\cdots\text{H}$, (e) $\text{C}\cdots\text{C}$, (f) $\text{C}\cdots\text{O}/\text{O}\cdots\text{C}$, (g) $\text{H}\cdots\text{N}/\text{N}\cdots\text{H}$, (h) $\text{C}\cdots\text{N}/\text{N}\cdots\text{C}$ and (i) $\text{N}\cdots\text{O}/\text{O}\cdots\text{N}$ interactions. The d_i and d_e values are the closest internal and external distances (in Å) from given points on the Hirshfeld surface contacts.

Table 2
Comparison (X-ray and DFT) of selected bond lengths and angles (Å, °).

Bonds/angles	X-ray	B3LYP/6-311G(d,p)
O1—C1	1.2288 (14)	1.2231
N1—C5	1.3993 (14)	1.3955
N1—C10	1.4742 (14)	1.4727
N1—C1	1.3774 (16)	1.4035
O2—C13	1.3123 (17)	1.3460
O2—C14	1.4491 (17)	1.4399
O3—C13	1.1955 (16)	1.2081
C5—C4	1.4159 (16)	1.4234
C5—C6	1.4011 (17)	1.4062
C4—C3	1.4516 (16)	1.4539
C4—C9	1.4064 (16)	1.4096
C5—N1—C10	120.18 (10)	120.925
C1—N1—C5	123.16 (9)	123.436
C1—N1—C10	116.52 (10)	115.623
C13—O2—C14	116.39 (12)	115.680
N1—C5—C4	120.23 (10)	120.142
N1—C5—C6	119.97 (10)	120.504
C6—C5—C4	119.80 (10)	119.355
C5—C4—C3	117.38 (10)	117.701
C9—C4—C5	118.06 (11)	118.477

shown in Fig. 4. The blue regions indicate positive electrostatic potential (hydrogen-bond donors), while the red regions indicate negative electrostatic potential (hydrogen-bond acceptors). The shape-index of the HS is a tool to visualize the π - π stacking interactions by the presence of adjacent red and blue triangles (Fig. 5). The overall two-dimensional fingerprint plot [Fig. 6(a)] and those delineated into H···H, H···C/C···H, H···O/O···H, C···C, C···O/O···C, H···N/N···H, C···N/N···C and N···O/O···N contacts (McKinnon *et al.*, 2007) are illustrated in Figs. 6(b)–(i), respectively, together with their relative contributions to the Hirshfeld surface. The most important interaction is H···H, contributing 36.0% to the overall crystal packing, which is reflected in Fig. 6(b) as widely scattered points of high density due to the large hydrogen content of the molecule with the tip at $d_e = d_i = 1.22$ Å. In the absence of C—H··· π interactions, the pair of characteristic wings resulting in the fingerprint plot delineated into H···C/C···H contacts [Fig. 6(c)] have a 28.9% contribution to the HS, with the tips at $d_e + d_i = 2.68$ Å. The pair of the scattered points of spikes resulting in the fingerprint plot delineated into

H···O/O···H contacts [Fig. 6(d)], with a 23.5% contribution to the HS, has an almost symmetric distribution of points, with the tips at $d_e + d_i = 2.44$ Å. The C···C contacts [Fig. 6(e)] appear as an arrow-shaped distribution of points and have a contribution of 7.0% to the HS with the tip at $d_e = d_i = 1.69$ Å. The tiny spikes of C···O/O···C contacts [Fig. 6(f)], with a 2.5% contribution to the HS, are visible at $d_e + d_i = 3.58$ Å. Finally, the H···N/N···H [Fig. 6(g)], C···N/N···C [Fig. 6(h)] and N···O/O···N [Fig. 6(i)] contacts contribute 1.4, 0.4 and 0.4%, respectively, to the HS.

The Hirshfeld surface representations with the function d_{norm} plotted onto the surface are shown for the H···H and H···C/C···H interactions in Figs. 7(a)–(c), respectively.

The Hirshfeld surface analysis confirms the importance of H-atom contacts in establishing the packing. The large number of H···H, H···C/C···H and H···O/O···H interactions suggest that van der Waals interactions play the major role in the crystal packing (Hathwar *et al.*, 2015).

5. Interaction energy calculations and energy frameworks

Using *CrystalExplorer* (Spackman *et al.*, 2021), the intermolecular interaction energies were calculated at the CEB3LYP/631G(d,p) energy level, where a cluster of molecules is generated by applying crystallographic symmetry operations with respect to a selected central molecule within a radius of 3.8 Å by default (Turner *et al.*, 2014). The total intermolecular energy (E_{tot}) is the sum of electrostatic (E_{ele}), polarization (E_{pol}), dispersion (E_{dis}) and exchange–repulsion (E_{rep}) energies (Turner *et al.*, 2015), with scale factors of 1.057, 0.740, 0.871 and 0.618, respectively (Mackenzie *et al.*, 2017). Energy frameworks combine the calculation of intermolecular interaction energies with a graphical representation of their magnitude (Turner *et al.*, 2015). Energies between molecular pairs are represented as cylinders joining the centroids of pairs of molecules with the cylinder radius proportional to the relative strength of the corresponding interaction energy. Energy frameworks were constructed for E_{ele} (red cylinders), E_{dis} (green cylinders) and E_{tot} (blue cylinders), and are shown in Figs. 8(a)–(c). The evaluation of the electrostatic, dispersion

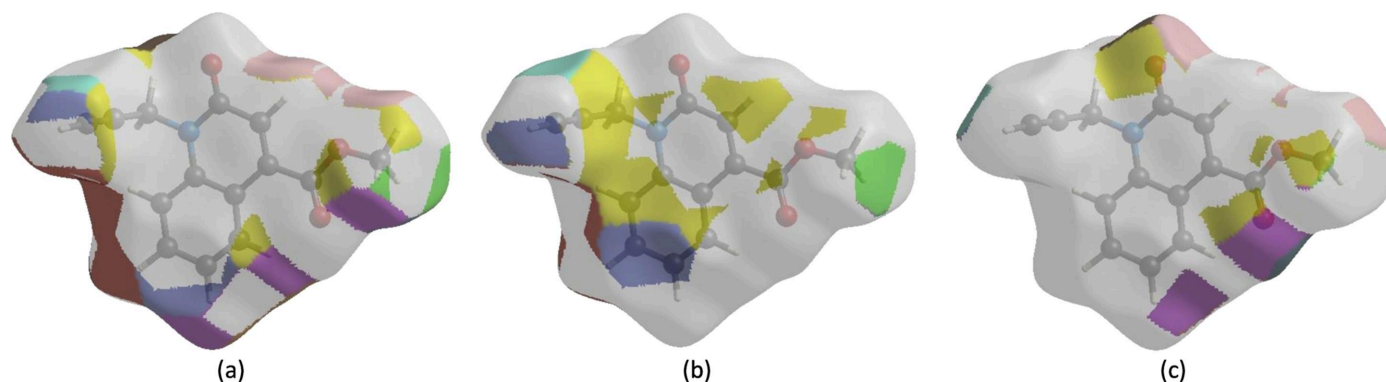


Figure 7
The Hirshfeld surface representations with the function d_{norm} plotted onto the surface for (a) H···H, (b) H···C/C···H and (c) H···O/O···H interactions.

Table 3

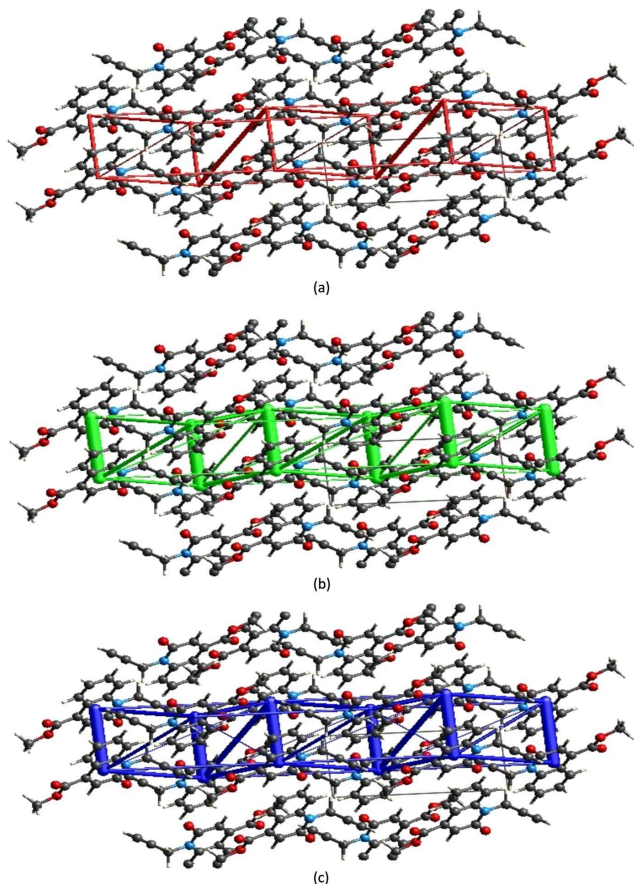
Calculated energies for compound (I).

Total energy, TE (eV)	-22331.1678
E_{HOMO} (eV)	-6.35
E_{LUMO} (eV)	-2.35
Gap, ΔE (eV)	-4.0
Dipole moment, μ (Debye)	2.1062
Ionization potential, I (eV)	6.35
Electron affinity, A	2.35
Electronegativity, χ	4.35
Hardness, η	2
Electrophilicity index, ω	4.73
Softness, σ	0.5
Fraction of electron transferred, ΔN	0.66

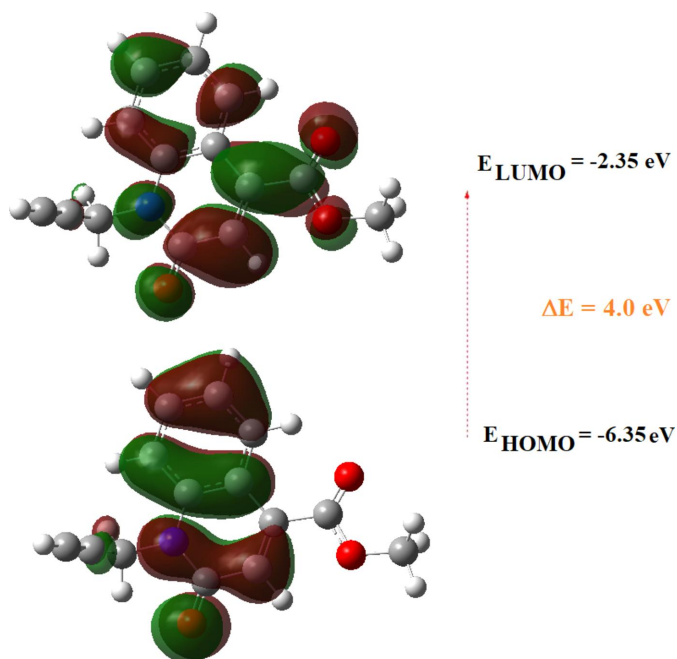
and total energy frameworks indicates that in the title compound the stabilization is dominated by the dispersion energy contribution.

6. DFT calculations

The optimized structure of the title compound in the gas phase was computed on the basis of density functional theory (DFT) using the standard B3LYP functional and the 6311G(d,p) basis


Figure 8

The energy frameworks, viewed down the c axis, for a cluster of molecules of the title compound, showing the (a) electrostatic energy, (b) dispersion energy and (c) total energy diagrams, where the b axis is vertical and the c axis is horizontal. The cylindrical radius is proportional to the relative strength of the corresponding energies and was adjusted to the same scale factor of 80 with a cut-off value of 5 kJ mol^{-1} within $2 \times 2 \times 2$ unit cells.


Figure 9

The energy band gap of the title compound.

set (Becke, 1993), as implemented in *GAUSSIAN09* (Frisch *et al.*, 2009). Comparisons of calculated bond lengths and angles with those of the experimental study are compiled in Table 2. The frontier orbitals were also investigated, and the highest occupied molecular orbital (HOMO) and lowest unoccupied molecular orbital (LUMO) orbitals are depicted in Fig. 9. It can be seen that the electron density of the HOMO is mostly distributed within the quinoline moiety, while that of the LUMO is mostly distributed over the carboxylate group.

Other chemistry descriptors (chemical hardness η , softness S , electronegativity χ and electrophilicity ω) derived from the conceptual DFT calculations are given in Table 3. The HOMO and LUMO are localized in the plane extending from the methyl 2-oxo-1-(prop-2-ynyl)-1,2-dihydroquinoline-4-carboxylate ring. The energy band gap [$\Delta E = E_{\text{LUMO}} - E_{\text{HOMO}}$] (Fig. 9) of the molecule is about -4.0 eV , with individual frontier molecular orbital energies, E_{HOMO} and E_{LUMO} , of -6.35 and -2.35 eV , respectively.

7. Database survey

A search of the Cambridge Structural Database (CSD, updated 20 March 2023; Groom *et al.*, 2016) using fragment (II) (Fig. 10) returned 20 hits, 16 of which contained an ester group attached to C7 (the rest contained an alkyl group at this position) and, only two of them, with refcodes ROKCIG (Filali Baba *et al.*, 2019) and REYREV (Filali Baba *et al.*, 2017), contain halogen atoms attached to aromatic rings. The former is more closely related to the title molecule due to the presence of an ethyl group on the nitrogen and ester substituents. Unlike the title molecule, that of ROKCIG forms an inverted dimer *via* C—H...O hydrogen bonds (instead of ribbons), with layer-by-layer connections approximately

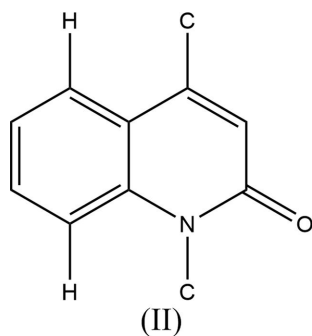


Figure 10

The molecular moiety used for the database search.

parallel to $(10\bar{4})$, but it has no C—H...Cl hydrogen bonds or π – π stacking interactions. The halogen-free analogue of ROKCIG (ROKCOM; Filali Baba *et al.*, 2019) uses C—H...O hydrogen bonds to form molecular bands along the *c* axis, which are connected by weak π – π interactions.

8. Refinement

Crystal, data collection and refinement details are presented in Table 4. H atoms were included as riding contributions in idealized positions with isotropic displacement parameters tied to those of the attached atoms. Two reflections obscured by the beamstop were omitted from the final refinement.

9. Synthesis and crystallization

To a solution of methyl 2-oxo-1,2-dihydroquinoline-4-carboxylate (4.47 mmol) in 10 ml of dimethylformamide (DMF) were added propargyl bromide (9.83 mmol), K_2CO_3 (22.36 mmol) and tetra-*n*-butylammonium bromide (TBAB; 0.5 mmol). The reaction mixture was stirred at room temperature in DMF for 6 h. After removal of the formed salts, the solvent was evaporated under reduced pressure and the residue obtained was dissolved in dichloromethane. The organic phase was dried over Na_2SO_4 and then concentrated *in vacuo*. A pure compound was obtained after recrystallization from dichloromethane/hexane (2:3 *v/v*).

Acknowledgements

TH is grateful to Hacettepe University Scientific Research Project Unit.

Funding information

Funding for this research was provided by: Hacettepe University Scientific Research Project Unit (grant No. 013 D04 602 004 to T. Hökelek).

References

Abdel-Wahab, B. F., Khidre, R. E., Farahat, A. A. & El-Ahl, A. S. (2012). *Arkivoc*, pp. 211–276.

Table 4

Experimental details.

Crystal data	
Chemical formula	$C_{14}H_{11}NO_3$
M_r	241.24
Crystal system, space group	Triclinic, $P\bar{1}$
Temperature (K)	296
<i>a</i> , <i>b</i> , <i>c</i> (Å)	4.7033 (2), 11.1113 (6), 11.3876 (5)
α , β , γ (°)	81.759 (2), 83.356 (2), 85.564 (2)
<i>V</i> (Å ³)	583.89 (5)
<i>Z</i>	2
Radiation type	Mo $K\alpha$
μ (mm ^{−1})	0.10
Crystal size (mm)	0.24 × 0.14 × 0.11
Data collection	
Diffractometer	Bruker DUO PHOTON III
Absorption correction	Multi-scan (<i>SADABS</i> ; Krause <i>et al.</i> , 2015)
T_{min} , T_{max}	0.708, 0.746
No. of measured, independent and observed [$I > 2\sigma(I)$] reflections	45341, 3559, 2489
R_{int}	0.045
$(\sin \theta/\lambda)_{max}$ (Å ^{−1})	0.714
Refinement	
$R[F^2 > 2\sigma(F^2)]$, $wR(F^2)$, <i>S</i>	0.047, 0.148, 1.11
No. of reflections	3559
No. of parameters	207
H-atom treatment	All H-atom parameters refined
$\Delta\rho_{max}$, $\Delta\rho_{min}$ (e Å ^{−3})	0.38, −0.28

Computer programs: *APEX3* and *SAINT* (Bruker, 2019), *SHELXT* (Sheldrick, 2015a), *SHELXL* (Sheldrick, 2015b) and *OLEX2* (Dolomanov *et al.*, 2009).

Baba, Y. F., Gökce, H., Rodi, Y. K., Hayani, S., Chahdi, F. O., Boukir, A., Jasinski, J. P., Kaur, M., Hökelek, T., Sebbar, N. K. & Essassi, E. M. (2020). *J. Mol. Struct.* **1217**, 128461.

Becke, A. D. (1993). *J. Chem. Phys.* **98**, 5648–5652.

Bouzian, Y., Hlimi, F., Sebbar, N. K., El Hafi, M., Hni, B., Essassi, E. M. & Mague, J. T. (2018). *IUCrData*, **3**, x181438.

Bruker (2019). *APEX3* and *SAINT*, Bruker AXS, Inc., Madison, Wisconsin, USA.

Dolomanov, O. V., Bourhis, L. J., Gildea, R. J., Howard, J. A. K. & Puschmann, H. (2009). *J. Appl. Cryst.* **42**, 339–341.

Filali Baba, Y., Elmsellem, H., Kandri Rodi, Y., Steli, H., Ouazzani Chahdi, F., Ouzidan, Y., Sebbar, N. K. & Essassi, E. M. (2016b). *Environ. Sci.* **7**, 2424–2434.

Filali Baba, Y., Elmsellem, H., Kandri Rodi, Y., Steli, H., Ouazzani Chahdi, F., Ouzidan, Y., Sebbar, N. K., Essassi, E. M., El-Hajjaji, F. & Hammouti, B. (2016a). *Pharm. Lett.* **8**, 128–137.

Filali Baba, Y., Kandri Rodi, Y., Ouzidan, Y., Mague, J. T., Ouazzani Chahdi, F. & Essassi, E. M. (2017). *IUCrData*, **2**, x171038.

Filali Baba, Y., Sert, Y., Kandri Rodi, Y., Hayani, S., Mague, J. T., Prim, D., Marrot, J., Ouazzani Chahdi, F., Sebbar, N. K. & Essassi, E. M. (2019). *J. Mol. Struct.* **1188**, 255–268.

Frisch, M. J., Trucks, G. W., Schlegel, H. B., Scuseria, G. E., Robb, M. A., Cheeseman, J. R., Scalmani, G., Barone, V., Mennucci, B., Petersson, G. A., Nakatsuji, H., Caricato, M., Li, X., Hratchian, H. P., Izmaylov, A. F., Bloino, J., Zheng, G., Sonnenberg, J. L., Hada, M., Ehara, M., Toyota, K., Fukuda, R., Hasegawa, J., Ishida, M., Nakajima, T., Honda, Y., Kitao, O., Nakai, H., Vreven, T., Montgomery, J. A. Jr, Peralta, J. E., Ogliaro, F., Bearpark, M., Heyd, J. J., Brothers, E., Kudin, K. N., Staroverov, V. N., Kobayashi, R., Normand, J., Raghavachari, K., Rendell, A., Burant, J. C., Iyengar, S. S., Tomasi, J., Cossi, M., Rega, N., Millam, J. M., Klene, M., Knox, J. E., Cross, J. B., Bakken, V., Adamo, C., Jaramillo, J., Gomperts, R., Stratmann, R. E., Yazyev, O., Austin, A. J., Cammi, R., Pomelli, C., Ochterski, J. W., Martin, R. L., Morokuma, K., Zakrzewski, V. G., Voth, G. A., Salvador, P., Dannenberg, J. J., Dapprich, S., Daniels,

- A. D., Farkas, O., Foresman, J. B., Ortiz, J. V., Cioslowski, J. & Fox, D. J. (2009). *GAUSSIAN09*. Gaussian Inc., Wallingford, CT, USA. <https://gaussian.com/>.
- Groom, C. R., Bruno, I. J., Lightfoot, M. P. & Ward, S. C. (2016). *Acta Cryst.* **B72**, 171–179.
- Hathwar, V. R., Sist, M., Jørgensen, M. R. V., Mamakhel, A. H., Wang, X., Hoffmann, C. M., Sugimoto, K., Overgaard, J. & Iversen, B. B. (2015). *IUCrJ*, **2**, 563–574.
- Hayani, S., Sert, Y., Baba, Y. F., Benhiba, F., Chahdi, F. O., Laraqui, F. Z., Mague, J. T., El Ibrahim, B., Sebbar, N. K., Rodi, Y. K. & Essassi, E. M. (2021). *J. Mol. Struct.* **1227**, 129520.
- Hirshfeld, H. L. (1977). *Theor. Chim. Acta*, **44**, 129–138.
- Hökelek, T., Dal, H., Tercan, B., Özbek, F. E. & Necefoğlu, H. (2009). *Acta Cryst.* **E65**, m607–m608.
- Jayatilaka, D., Grimwood, D. J., Lee, A., Lemay, A., Russel, A. J., Taylor, C., Wolff, S. K., Cassam-Chenai, P. & Whitton, A. (2005). *TONTO – A System for Computational Chemistry*. Available at: <http://hirshfeldsurface.net/>.
- Katoh, M., Matsune, R., Nagase, H. & Honda, T. (2004). *Tetrahedron Lett.* **45**, 6221–6223.
- Krause, L., Herbst-Irmer, R., Sheldrick, G. M. & Stalke, D. (2015). *J. Appl. Cryst.* **48**, 3–10.
- Leatham, P. A., Bird, H. A., Wright, V., Seymour, D. & Gordon, A. (1983). *J. Rheumatol. Inflamm.* **6**, 209–211.
- Mackenzie, C. F., Spackman, P. R., Jayatilaka, D. & Spackman, M. A. (2017). *IUCrJ*, **4**, 575–587.
- Mahamoud, A., Chevalier, J., Davin-Regli, A., Barbe, J. & Pages, J. (2006). *Curr. Drug Targets*, **7**, 843–847.
- McKinnon, J. J., Jayatilaka, D. & Spackman, M. A. (2007). *Chem. Commun.* pp. 3814–3816.
- Muruganantham, N., Sivakumar, R., Anbalagan, N., Gunasekaran, V. & Leonard, J. T. (2004). *Biol. Pharm. Bull.* **27**, 1683–1687.
- Sheldrick, G. M. (2015a). *Acta Cryst.* **A71**, 3–8.
- Sheldrick, G. M. (2015b). *Acta Cryst.* **C71**, 3–8.
- Sim, G. A., Robertson, J. M. & Goodwin, T. H. (1955). *Acta Cryst.* **8**, 157–164.
- Spackman, M. A., McKinnon, J. J. & Jayatilaka, D. (2008). *Cryst. EngComm*, **10**, 377–388.
- Spackman, P. R., Turner, M. J., McKinnon, J. J., Wolff, S. K., Grimwood, D. J., Jayatilaka, D. & Spackman, M. A. (2021). *J. Appl. Cryst.* **54**, 1006–1011.
- Strekowski, L., Mokrosz, J. L., Honkan, V. A., Czarny, A., Cegla, M. T., Wydra, R. L., Patterson, S. E. & Schinazi, R. F. (1991). *J. Med. Chem.* **34**, 1739–1746.
- Turner, M. J., Grabowsky, S., Jayatilaka, D. & Spackman, M. A. (2014). *J. Phys. Chem. Lett.* **5**, 4249–4255.
- Turner, M. J., Thomas, S. P., Shi, M. W., Jayatilaka, D. & Spackman, M. A. (2015). *Chem. Commun.* **51**, 3735–3738.
- Venkatesan, P., Thamocharan, S., Ilangovan, A., Liang, H. & Sundius, T. (2016). *Spectrochim. Acta A Mol. Biomol. Spectrosc.* **153**, 625–636.
- Wilson, W. D., Zhao, M., Patterson, S. E., Wydra, R. L., Janda, L., Streckowski, L. & Schinazi, R. F. (1992). *J. Med. Chem.* **2**, 102–110.

supporting information

Acta Cryst. (2023). E79, 883-889 [https://doi.org/10.1107/S2056989023007557]

Crystal structure, Hirshfeld surface analysis, interaction energy and energy framework calculations, as well as density functional theory (DFT) computation, of methyl 2-oxo-1-(prop-2-ynyl)-1,2-dihydroquinoline-4-carboxylate

Ayoub El-Mrabet, Amal Haoudi, Samira Dalbouha, Mohamed Khalid Skalli, Tuncer Hökelek, Frederic Capet, Youssef Kandri Rodi, Ahmed Mazzah and Nada Kheira Sebbar

Computing details

Data collection: *APEX3* (Bruker, 2019); cell refinement: *SAINTE* (Bruker, 2019); data reduction: *SAINTE* (Bruker, 2019); program(s) used to solve structure: *SHELXT* (Sheldrick, 2015a); program(s) used to refine structure: *SHELXL* (Sheldrick, 2015b); molecular graphics: *OLEX2* (Dolomanov *et al.*, 2009); software used to prepare material for publication: *OLEX2* (Dolomanov *et al.*, 2009).

Methyl 2-oxo-1-(prop-2-ynyl)-1,2-dihydroquinoline-4-carboxylate

Crystal data

$C_{14}H_{11}NO_3$	$Z = 2$
$M_r = 241.24$	$F(000) = 252$
Triclinic, $P\bar{1}$	$D_x = 1.372 \text{ Mg m}^{-3}$
$a = 4.7033 (2) \text{ \AA}$	Mo $K\alpha$ radiation, $\lambda = 0.71073 \text{ \AA}$
$b = 11.1113 (6) \text{ \AA}$	Cell parameters from 9957 reflections
$c = 11.3876 (5) \text{ \AA}$	$\theta = 2.4\text{--}30.2^\circ$
$\alpha = 81.759 (2)^\circ$	$\mu = 0.10 \text{ mm}^{-1}$
$\beta = 83.356 (2)^\circ$	$T = 296 \text{ K}$
$\gamma = 85.564 (2)^\circ$	Block, colourless
$V = 583.89 (5) \text{ \AA}^3$	$0.24 \times 0.14 \times 0.11 \text{ mm}$

Data collection

Bruker DUO PHOTON III diffractometer	2489 reflections with $I > 2\sigma(I)$
Radiation source: microfocus sealed X-ray tube	$R_{\text{int}} = 0.045$
φ and ω scans	$\theta_{\text{max}} = 30.5^\circ$, $\theta_{\text{min}} = 1.8^\circ$
Absorption correction: multi-scan (SADABS; Krause <i>et al.</i> , 2015)	$h = -6 \rightarrow 6$
$T_{\text{min}} = 0.708$, $T_{\text{max}} = 0.746$	$k = -15 \rightarrow 15$
45341 measured reflections	$l = -16 \rightarrow 16$
3559 independent reflections	3 standard reflections every 1000 reflections
	intensity decay: 1%

*Refinement*Refinement on F^2

Least-squares matrix: full

 $R[F^2 > 2\sigma(F^2)] = 0.047$ $wR(F^2) = 0.148$ $S = 1.11$

3559 reflections

207 parameters

0 restraints

Primary atom site location: dual

Secondary atom site location: difference Fourier map

Hydrogen site location: difference Fourier map

All H-atom parameters refined

 $w = 1/[\sigma^2(F_o^2) + (0.0712P)^2 + 0.064P]$ where $P = (F_o^2 + 2F_c^2)/3$ $(\Delta/\sigma)_{\max} < 0.001$ $\Delta\rho_{\max} = 0.38 \text{ e } \text{\AA}^{-3}$ $\Delta\rho_{\min} = -0.28 \text{ e } \text{\AA}^{-3}$ *Special details*

Geometry. All esds (except the esd in the dihedral angle between two l.s. planes) are estimated using the full covariance matrix. The cell esds are taken into account individually in the estimation of esds in distances, angles and torsion angles; correlations between esds in cell parameters are only used when they are defined by crystal symmetry. An approximate (isotropic) treatment of cell esds is used for estimating esds involving l.s. planes.

Fractional atomic coordinates and isotropic or equivalent isotropic displacement parameters (\AA^2)

	<i>x</i>	<i>y</i>	<i>z</i>	$U_{\text{iso}}^*/U_{\text{eq}}$
O1	0.3589 (2)	0.16022 (9)	0.53718 (9)	0.0571 (3)
N1	0.6716 (2)	0.14916 (9)	0.67741 (9)	0.0381 (2)
O2	0.2219 (3)	0.56421 (9)	0.64710 (10)	0.0655 (3)
O3	0.3962 (3)	0.56270 (10)	0.81846 (12)	0.0812 (4)
C5	0.7779 (2)	0.19819 (10)	0.76892 (10)	0.0359 (2)
C4	0.6875 (2)	0.31800 (10)	0.79156 (10)	0.0357 (2)
C3	0.4848 (3)	0.38599 (10)	0.71625 (10)	0.0372 (3)
C10	0.7636 (3)	0.02397 (11)	0.65470 (13)	0.0441 (3)
C13	0.3695 (3)	0.51328 (11)	0.73414 (12)	0.0434 (3)
C11	0.6261 (3)	-0.06721 (11)	0.74351 (13)	0.0463 (3)
C6	0.9724 (3)	0.12821 (12)	0.83921 (12)	0.0439 (3)
C1	0.4663 (3)	0.20952 (11)	0.60989 (11)	0.0411 (3)
C2	0.3857 (3)	0.33419 (11)	0.63055 (11)	0.0422 (3)
C9	0.8005 (3)	0.36311 (12)	0.88452 (12)	0.0438 (3)
C8	0.9935 (3)	0.29352 (14)	0.95173 (12)	0.0500 (3)
C7	1.0789 (3)	0.17610 (14)	0.92919 (13)	0.0497 (3)
C12	0.5140 (4)	-0.14126 (14)	0.81495 (17)	0.0605 (4)
C14	0.0863 (5)	0.68407 (15)	0.6591 (2)	0.0686 (5)
H10A	0.720 (4)	0.0174 (14)	0.5791 (15)	0.053 (4)*
H9	0.736 (3)	0.4439 (15)	0.9029 (14)	0.054 (4)*
H10B	0.974 (3)	0.0129 (13)	0.6502 (12)	0.044 (4)*
H6	1.030 (3)	0.0475 (15)	0.8245 (14)	0.052 (4)*
H2	0.247 (4)	0.3772 (15)	0.5795 (15)	0.056 (4)*
H8	1.067 (4)	0.3254 (16)	1.0161 (17)	0.070 (5)*
H7	1.214 (4)	0.1274 (17)	0.9743 (16)	0.066 (5)*
H14A	0.232 (6)	0.741 (2)	0.657 (2)	0.111 (8)*
H14B	-0.011 (5)	0.7061 (19)	0.590 (2)	0.083 (6)*
H14C	-0.036 (6)	0.684 (2)	0.729 (2)	0.100 (8)*
H12	0.435 (5)	-0.201 (2)	0.874 (2)	0.091 (7)*

Atomic displacement parameters (\AA^2)

	U^{11}	U^{22}	U^{33}	U^{12}	U^{13}	U^{23}
O1	0.0699 (7)	0.0505 (6)	0.0589 (6)	0.0021 (5)	-0.0237 (5)	-0.0248 (5)
N1	0.0416 (5)	0.0328 (5)	0.0416 (5)	0.0006 (4)	-0.0036 (4)	-0.0131 (4)
O2	0.0899 (8)	0.0451 (6)	0.0658 (7)	0.0234 (5)	-0.0303 (6)	-0.0185 (5)
O3	0.1245 (11)	0.0485 (6)	0.0815 (8)	0.0261 (6)	-0.0469 (8)	-0.0339 (6)
C5	0.0346 (5)	0.0359 (6)	0.0379 (6)	-0.0031 (4)	-0.0010 (4)	-0.0092 (4)
C4	0.0357 (5)	0.0355 (6)	0.0367 (5)	-0.0027 (4)	-0.0009 (4)	-0.0097 (4)
C3	0.0401 (6)	0.0323 (5)	0.0395 (6)	-0.0015 (4)	-0.0015 (4)	-0.0083 (4)
C10	0.0468 (7)	0.0369 (6)	0.0508 (7)	0.0033 (5)	-0.0026 (5)	-0.0189 (5)
C13	0.0488 (7)	0.0337 (6)	0.0488 (7)	-0.0004 (5)	-0.0053 (5)	-0.0097 (5)
C11	0.0466 (7)	0.0352 (6)	0.0607 (8)	0.0035 (5)	-0.0097 (6)	-0.0185 (6)
C6	0.0423 (6)	0.0402 (6)	0.0491 (7)	0.0027 (5)	-0.0061 (5)	-0.0075 (5)
C1	0.0461 (6)	0.0387 (6)	0.0407 (6)	-0.0015 (5)	-0.0056 (5)	-0.0125 (5)
C2	0.0485 (7)	0.0368 (6)	0.0425 (6)	0.0022 (5)	-0.0101 (5)	-0.0085 (5)
C9	0.0460 (6)	0.0440 (7)	0.0447 (6)	-0.0034 (5)	-0.0051 (5)	-0.0161 (5)
C8	0.0501 (7)	0.0602 (8)	0.0438 (7)	-0.0047 (6)	-0.0105 (6)	-0.0154 (6)
C7	0.0454 (7)	0.0572 (8)	0.0472 (7)	0.0010 (6)	-0.0119 (6)	-0.0055 (6)
C12	0.0642 (9)	0.0447 (8)	0.0737 (10)	-0.0063 (7)	-0.0086 (8)	-0.0093 (7)
C14	0.0861 (13)	0.0412 (8)	0.0810 (12)	0.0209 (8)	-0.0280 (11)	-0.0148 (8)

Geometric parameters (\AA , $^\circ$)

O1—C1	1.2288 (14)	C10—H10B	0.983 (15)
N1—C5	1.3993 (14)	C11—C12	1.180 (2)
N1—C10	1.4742 (14)	C6—C7	1.3785 (19)
N1—C1	1.3774 (16)	C6—H6	0.949 (17)
O2—C13	1.3123 (17)	C1—C2	1.4524 (17)
O2—C14	1.4491 (17)	C2—H2	0.977 (18)
O3—C13	1.1955 (16)	C9—C8	1.3750 (19)
C5—C4	1.4159 (16)	C9—H9	0.969 (17)
C5—C6	1.4011 (17)	C8—C7	1.386 (2)
C4—C3	1.4516 (16)	C8—H8	0.966 (19)
C4—C9	1.4064 (16)	C7—H7	0.950 (19)
C3—C13	1.5081 (16)	C12—H12	0.94 (2)
C3—C2	1.3449 (17)	C14—H14A	0.97 (3)
C10—C11	1.457 (2)	C14—H14B	0.95 (2)
C10—H10A	0.922 (16)	C14—H14C	0.93 (3)
C5—N1—C10	120.18 (10)	C7—C6—C5	120.28 (12)
C1—N1—C5	123.16 (9)	C7—C6—H6	120.2 (9)
C1—N1—C10	116.52 (10)	O1—C1—N1	121.71 (11)
C13—O2—C14	116.39 (12)	O1—C1—C2	122.56 (12)
N1—C5—C4	120.23 (10)	N1—C1—C2	115.73 (10)
N1—C5—C6	119.97 (10)	C3—C2—C1	123.09 (11)
C6—C5—C4	119.80 (10)	C3—C2—H2	121.9 (10)
C5—C4—C3	117.38 (10)	C1—C2—H2	114.9 (10)

C9—C4—C5	118.06 (11)	C4—C9—H9	119.0 (10)
C9—C4—C3	124.56 (11)	C8—C9—C4	121.30 (12)
C4—C3—C13	121.83 (10)	C8—C9—H9	119.6 (10)
C2—C3—C4	120.15 (10)	C9—C8—C7	120.08 (12)
C2—C3—C13	117.97 (11)	C9—C8—H8	120.2 (11)
N1—C10—H10A	106.8 (10)	C7—C8—H8	119.7 (11)
N1—C10—H10B	109.5 (8)	C6—C7—C8	120.47 (13)
C11—C10—N1	112.13 (10)	C6—C7—H7	118.6 (11)
C11—C10—H10A	111.3 (10)	C8—C7—H7	120.9 (11)
C11—C10—H10B	111.7 (8)	C11—C12—H12	176.4 (14)
H10A—C10—H10B	105.1 (13)	O2—C14—H14A	109.5 (16)
O2—C13—C3	111.85 (10)	O2—C14—H14B	105.1 (13)
O3—C13—O2	122.55 (12)	O2—C14—H14C	111.5 (16)
O3—C13—C3	125.54 (12)	H14A—C14—H14B	107.6 (19)
C12—C11—C10	179.65 (16)	H14A—C14—H14C	110 (2)
C5—C6—H6	119.5 (9)	H14B—C14—H14C	113 (2)
O1—C1—C2—C3	174.62 (13)	C10—N1—C5—C4	-179.38 (10)
N1—C5—C4—C3	-0.33 (16)	C10—N1—C5—C6	0.02 (17)
N1—C5—C4—C9	179.99 (10)	C10—N1—C1—O1	2.22 (18)
N1—C5—C6—C7	179.74 (11)	C10—N1—C1—C2	-177.92 (10)
N1—C1—C2—C3	-5.23 (19)	C13—C3—C2—C1	-175.93 (11)
C5—N1—C10—C11	75.59 (14)	C6—C5—C4—C3	-179.73 (10)
C5—N1—C1—O1	-173.59 (11)	C6—C5—C4—C9	0.59 (17)
C5—N1—C1—C2	6.27 (18)	C1—N1—C5—C4	-3.71 (17)
C5—C4—C3—C13	178.69 (10)	C1—N1—C5—C6	175.68 (11)
C5—C4—C3—C2	1.31 (17)	C1—N1—C10—C11	-100.36 (13)
C5—C4—C9—C8	0.10 (19)	C2—C3—C13—O2	-11.40 (17)
C5—C6—C7—C8	0.4 (2)	C2—C3—C13—O3	165.96 (15)
C4—C5—C6—C7	-0.86 (19)	C9—C4—C3—C13	-1.66 (18)
C4—C3—C13—O2	171.16 (11)	C9—C4—C3—C2	-179.04 (12)
C4—C3—C13—O3	-11.5 (2)	C9—C8—C7—C6	0.3 (2)
C4—C3—C2—C1	1.54 (19)	C14—O2—C13—O3	-1.1 (2)
C4—C9—C8—C7	-0.5 (2)	C14—O2—C13—C3	176.33 (15)
C3—C4—C9—C8	-179.56 (12)		

Hydrogen-bond geometry (\AA , $^\circ$)

$D-H\cdots A$	$D-H$	$H\cdots A$	$D\cdots A$	$D-H\cdots A$
C9—H9 \cdots O3	0.969 (17)	2.210 (15)	2.8807 (19)	125.3 (12)
C10—H10A \cdots O1	0.922 (16)	2.277 (17)	2.6961 (17)	107.1 (12)
C14—H14B \cdots O1 ⁱ	0.95 (2)	2.56 (2)	3.433 (2)	153.8 (18)

Symmetry code: (i) $-x, -y+1, -z+1$.